Nuclear Engineering and Technology 54 (2022) 3415–3421

Contents lists available at ScienceDirect

Nuclear Engineering and Technology

journal homepage: www.elsevier.com/locate/net

Original Article

Impact of geometrical parameters on SGEMP responses in cylinder model

Jian-Nan Chen [a, *], Jun-Jie Zhang [a]

[a] Northwest Institute of Nuclear Technology, Xi'an, 710024, China

ARTICLE INFO

Article history:
Received 5 December 2021
Received in revised form
23 March 2022
Accepted 25 April 2022
Available online 2 May 2022

Keywords:
Geometrical parameter
SGEMP
Scaling law
Particle distribution
Cylinder model

ABSTRACT

This paper is aimed to find out the impact of the geometrical parameters, mainly the radius and the height of a cylinder, on the SGEMP response including the famous scaling law in the classical cylinder model using a homemade PIC code UNIPIC-3D. We computed the electric fields at the center and at the edge on the emission head face with different radii and heights under normal X-rays incidence. The results show that the electric field will increase with the radius but decrease with the height. We analyze the scaling law that links the electric field product and fluence product, and whereafter an irreconcilable contradiction raises when the radius is changeable, which limits the application range of the scaling law. Moreover, the field-height-radius relation is found and described by a combination of logarithmic and minus one-quarter numerical fitting law firstly. Particle and magnetic field distributions are used to explain all the behaviors of the fields reasonably. All the findings will assist the evaluation of SGEMP response in spacecraft protection.

1. Introduction

High-energy and huge-fluence X-rays and γ-rays from the high-altitude nuclear burst will act on the space vehicles and knock the photoelectrons and Compton electrons out with energies over **keV** magnitude via photoelectric effect and Compton scattering [1,2]. The space vehicles usually work at the outer space where the air can be ignored and the radiated X-rays there contain around 70%–85% energy of the total nuclear chain reaction while the γ-rays occupy no more than 0.5% in principle [1]. As a result, X-rays play a more important role in nuclear-explosion space-radiation effect than γ-rays. The injected electrons form a large space current from the emission surface, leading to the unbalance of electric potential on the vehicles and then causing enormous skin currents. The large space current and skin current stimulate the so-called system generated electromagnetic pulse (SGEMP) of which electric field could exceed 10^5 V m^{-1}, disturbing and even damaging the electronic systems in the space vehicles [3]. Thus, it is still worthy studying SGEMP responses and finding out more efficient ways to harden the space vehicles under high-energy rays in detail.

Lack of such high-energy radiation environment from a large space scale, for example, the true nuclear explosion source, other alternative equivalent methods have appeared. Analysis is the basic method and has obtained many useful conclusions in the early stage of studies [4–6]. However, as SGEMP responses are nonlinear in most conditions [7,8], analysis will not gain the ideal results at all the time. Therefore, the experiments in labs have been proceeded by the high-energy rays derived from the particle accelerator [9] or high-power lasers [10] instead. Nevertheless, the expensive cost and the uncertainty of the experiments will limit the study in consumption of time and efficiency. Along with the improvement of computer in recent decades, numerical simulation has developed to be an important method to research the nuclear-explosion electromagnetic effects [11–15], and the application of giant computer has extended it greatly into a larger computation space and increased the computation accuracy to a great extent. What's more, the non-negligible self-consistent effect between the moving particles and self-generated fields is able to be included without a mass of efforts in this way.

Particle-in-cell (PIC) method which could solve the self-consistent problem automatically has been developed for many years. It has the advantage of less computation resources and has been perfectly adapted in Linux system on the giant computer. Different kinds of PIC codes have been exploited, for example, MAGIC [16], XOOPIC [17], CHIPIC [18] and UNIPIC. The last one is our homemade code, which has been widely applied to the field of

* Corresponding author.
E-mail address: chennn1994@alumni.sjtu.edu.cn (J.-N. Chen).

https://doi.org/10.1016/j.net.2022.04.018

vacuum electronic device, such as studying the physical phenomena in diode [19,20], modeling the dielectric breakdown [21] and designing the high power microwave device [22]. Recently, it has been improved to handle the generation of EMP with good convenience [23–26]. Though the existent of air may bring great impact on the generation of electromagnetic fields [27], we could ignore it considering the flight altitude of the satellites.

However, even though PIC method takes the advantage of saving computation resources comparably over other ways, still lots of time will it consume [23]. In that case, plenty of researches have been carried out to study and summarize the responses of SGEMP under different inputs, such as the energy spectrum, pulse width, incident angle of the radiations, and the geometrical models of the irradiated object [28,29]. For convenience, the cylinder was considered a simplified model to stand for the traditional space vehicle roughly, and subsequently A. J. Woods brought a general descriptions of the scaling laws for SGEMP responses in that model, from which we could obtain the approximate electric field and surface current easily rather than the elaborate but time-consuming numerical simulation under a given input condition, and researchers have widely adopted it to verify their codes [24,30].

From a large range of studies, we know that the dimensional factor can inevitably change the results when the model converts from 2D to 3D. Likewise, the above-mentioned scaling law has some shortages when solving the changeable geometrical parameters, i.e., radius and height of the cylinder. As a result, we employed UNIPIC to make the question clear in this article. Section 2 briefly introduced the computational method and model. Section 3 presents the problem in Woods's scaling law and we analyze its shortcomings in depth. Then we introduce the height of the cylinder as another geometrical factor, explain how and why the electric field varies with it and ultimately come up with an overall fitting formula, linking the electric field, height and radius together. Section 4 summarizes this work.

2. Computation method and model

UNIPIC-3D is a fully electromagnetic PIC code, which is widely utilized to model the motion of the injection particles and compute the generation and propagation of the electromagnetic fields by combining time-dependent Maxwell's equations and Newton-Lorentz force equations. The differential form of Maxwell's equations field propagation part is as

$$\varepsilon\frac{\partial \mathbf{E}}{\partial t}=\nabla\times\mathbf{H}-\mathbf{J} \tag{1}$$

$$\frac{\partial \mathbf{B}}{\partial t}=-\nabla\times\mathbf{E} \tag{2}$$

where **E** and **H** are the electric field and magnetic field, ε and μ denote the permittivity and permeability of the medium, and **J** represents the electric current density. The Newton-Lorentz force equations can then be updated with the known **E** and **B** from Eqs. (1) and (2) to output the positions and velocities of particles as

$$\frac{\mathrm{d}}{\mathrm{d}t}\gamma m\boldsymbol{v}=q(\mathbf{E}+\boldsymbol{v}\times\mathbf{B}) \tag{3}$$

$$\frac{\mathrm{d}}{\mathrm{d}t}\boldsymbol{x}=\boldsymbol{v} \tag{4}$$

where m, q, $\boldsymbol{v}$ and $\boldsymbol{x}$ are the mass, charge, velocity and displacement of the electron separately, and the relativistic factor γ is expressed as

$$\gamma=\frac{1}{\sqrt{1-(v/c)^2}}=\sqrt{1+(u/c)^2} \tag{5}$$

where c is the speed of light, $\boldsymbol{u}=\gamma\boldsymbol{v}$.

Meanwhile, the conformal technique has been maturely combined in our code [23] with the partially filled cells (PFC) [31] approach. Compared with the first-order conventional staircased meshes, the PFC approach is capable to increase the accuracy of the boundary approximation with a second-order accuracy while reserving the benefits of the conventional algorithms. The symplectic integrator (SI) is employed here in order to provide a high order algorithm to simulate the dynamics of electromagnetic fields in time and second-order accurate in space, which can greatly decrease the numerical instability [32]. By using SI, Eqs. (1) and (2) can be expressed as follows,

$$\boldsymbol{E}^{n+(j+1)/r}=\boldsymbol{E}^{n+j/r}+\tilde{b}_j\Delta t\frac{1}{\varepsilon}\left(\frac{1}{\mu}\nabla\times\boldsymbol{B}^{n+(j+1)r}-\boldsymbol{J}^{n+(j+1)/r}\right) \tag{6}$$

$$\mathbf{B}^{n+(j+1)/r}=\mathbf{B}^{n+j/r}-b_j\Delta t\cdot\nabla\times\mathbf{E}^{n+r} \tag{7}$$

where, $j=0,\ldots,r$-1, b_j and $\tilde{b}_j$ are the coefficients for the explicit partitioned Runge-Kutta algorithm, r is the order of the method [23,33]. Then, we establish the foundation to simulate the electromagnetic field and particle distribution in complicated 3D models.

Calculations are performed for the response of a cylinder with radius R and height h illuminated on one head face by a batch of uniform X-rays pulse of energy fluence Φ, as shown in Fig. 1. The classical time history is proportional to the peak-normalized sine-squared profile Eq. (8) of which the rise time and full width at half maximum (FWHM) are equal [28],

$$I(t)=\sin^2\left(\frac{\pi t}{2\tau}\right) \tag{8}$$

where FWHM $\tau=25$ ns.

$$c\Delta t\le\frac{1}{\sqrt{\frac{1}{(\Delta x)^2}+\frac{1}{(\Delta y)^2}+\frac{1}{(\Delta z)^2}}}$$

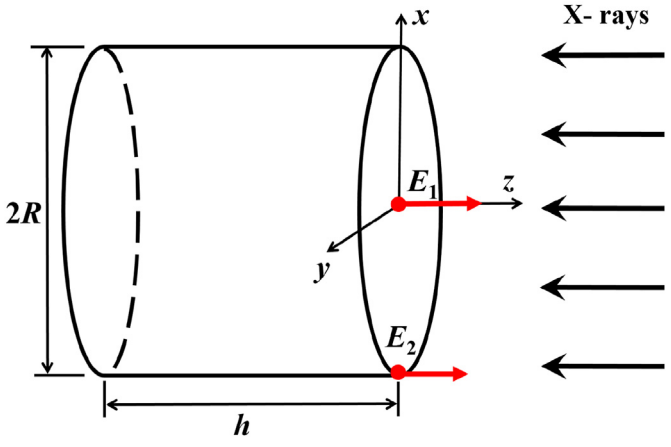

Fig. 1. Computation model. The X-rays irradiate on one head face uniformly along the $-z$ axis. The radius of the aluminum cylinder is R, and the height of the cylinder is h.

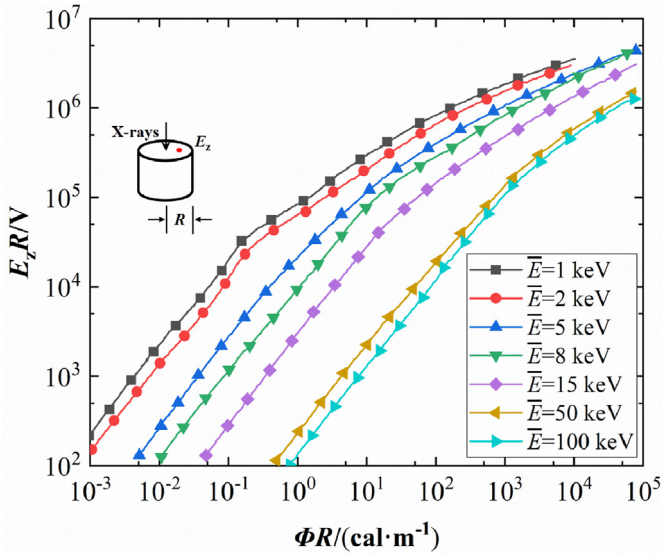

Fig. 2. The scaling law of normal electric field product E_zR vs. fluence product ΦR under different characterized energies in Ref. [28]. The normal electric field E_z is on the emission surface, R is the radius of the cylinder and fluence Φ is the energy fluence of the incident X-rays.

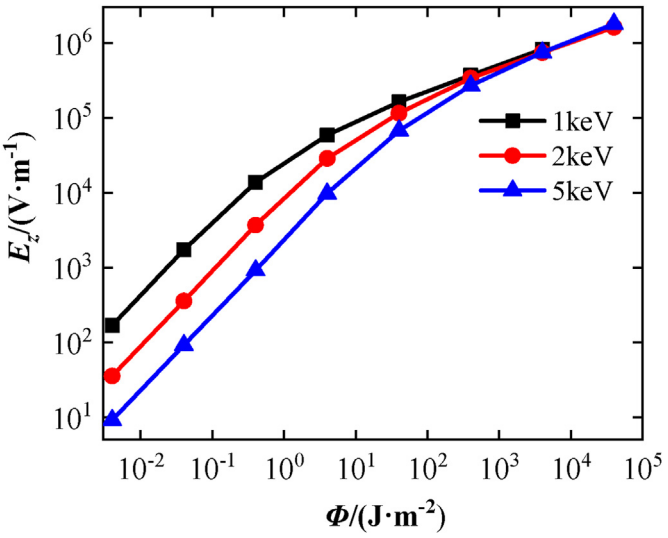

Fig. 3. Normal electric field E_z vs. energy fluence Φ under three characterized energies, $T = 1$ keV, $T = 2$ keV and $T = 5$ keV, when the radius of the cylinder $R = 0.1$ m, and the height of the cylinder $h = 0.2$ m by UNIPIC-3D.

The material of the cylinder model is set aluminum which is regarded as a perfect electric conductor. The X-rays usually obey the blackbody energy distribution with a characterized temperature T. From Ref. [34] we can acquire the electron emission parameters by the Monte Carlo code MCNP that the photoelectron yield of external emission surface is as a function of the characterized temperature, the emission angle submits to the cosine distribution, and the peak-normalized energy spectrum of the emission electron is expressed as Eq. (9),

$$f(E) = \exp(-E/T) \tag{9}$$

where E is the electron energy.

The free space domain is set at least twice along x axis and y axis and three times along z axis as large as the computational models, so that the reflected waves from the CPML boundary would influence the results less. The computational grids are all uniform cubes with $\triangle x \times \triangle y \times \triangle z = 0.01$ m $\times$ 0.01 m $\times$ 0.01 m, and the time step $\triangle t$ obeys the Courant stability condition.

$$c\Delta t \le \frac{1}{\sqrt{\frac{1}{(\Delta x)^2}+\frac{1}{(\Delta y)^2}+\frac{1}{(\Delta z)^2}}} \tag{10}$$

3. Results and discussion

3.1. SGEMP scaling law

It has been mentioned in section I that the scaling law in Ref. [28] is used to simplify the acquirement of the SGEMP response in a cylinder model. The relations between E_zR (electric field product at the top of the cylinder) and ΦR (fluence product) under incident X-rays of different blackbody characterized temperatures (or spectra with characteristic energies) are exhibited in Fig. 2. We have also employed UNIPIC-3D to simulate how the normal electric field E_z varies with the incident fluence Φ in a specific model of which radius $R = 0.1$ m, and height $h = 0.2$ m. The relation is indicated in Fig. 3 then.

Comparing Figs. 2 and 3, we can find the similar feature that below certain fluence threshold of each curve, E_zR (or E_z) changes with ΦR (or Φ) linearly, while the relation becomes sublinear beyond the threshold. This nonlinear relation is caused by the space-charge limited effect [24] which restricts both the currents and fields. These relations in the two figures are the same when the radius is constant, but when it comes to a changeable radius, the conclusion is significantly different.

3.2. Problems in the scaling law

The following is aimed to reveal why the above-mentioned relation is not universally adoptable. At the beginning, we need to know how the peak of the two normal electric field E_z changes with the radius R when the height of the cylinder is fixed. We choose $h = 0.1$ m unchangeably here, and the irradiation energy fluence is $\Phi = 0.4\ \mathrm{J\ m^{-2}}$, which supplies a low space-charge limited environment. E_1 is the electric field at the center on the emission surface and E_2 is at the edge, pointed out in Fig. 1. As we can see, both the two electric fields are growing with radius. When the radius is small (around no more than 0.2 m), two electric fields increase nearly linearly. Nevertheless, at the time the radius exceeds some threshold, sublinear increase occurs likewise. It is also indicated that E_2 is conspicuously larger than E_1 for all the radii because of the edge-effect [20] due to the repulsive forces among the electrons on and above the emission surface.

Then, we map the particle distributions above the emission surface with $R = 0.2$ m at different times so as to dig for the reason why the tendency between the electric field and radius is positive correlation. As we know, the pulsed electric field is generated by the moving electrons, and its strength depends mainly on the local electron density. Usually, at the beginning of the injection, electrons will just cover the emission surface, as shown in Fig. 5(a). However, as time passes by, because of not only the cosine emission angle, but also the repulsive forces among the electrons, from Fig. 5(b) it is indicated that the emission electrons are going to spread around transversely and symmetrically, and the electron-coverage area could be four times as large as that in Fig. 5(a). Due to the above spread statement, the electron density may decrease as a result. Hence, the electric field strength is actually determined

by the electron accumulation, that is how many electrons generate or move from the other areas to the area of interest and how soon the electrons there spread around.

Now, let us focus on the electric fields on the emission surface. The electron generation rate and spread speed are nearly not influenced by the size of the radius, and then it is the quantity of electrons moving from other areas that impact the electric field. When the radius is small, the total emission area is small, which results in a limited number of the electrons that could transport to the diagnostic point, and the number of those will increase as the radius, i.e., the total emission area grows larger. So, that accounts for the increasing relation that electric fields grow with the radius in Fig. 4. However, when the number of electrons is large enough, the local electrons have the ability to impede and block the other electrons which are farther from the diagnostic point. Therefore, no matter how larger the radius increases, the blocked electrons will not influence the electric field of interest anymore, which leads to the saturation electric field at the steady part in Fig. 4.

Now, the contradiction appears. Firstly, let us think about this question that how the electric field product E_zR will change with the fluence product ΦR in the linear stage with a settled radius in Fig. 2. From Fig. 3 we know the answer is linear increase for sure. However, once we fix the value of energy fluence Φ and increase the value of radius R only, what is the answer then? If electric fields don't change with radius, then we could obtain Fig. 2 from multiplying R by E_z in Fig. 3 obviously. But Fig. 4 tells us that normal electric fields will be enlarged unfortunately. Thus, for an original condition A with fluence product $\Phi_A R_A$ and electric field product $E_A R_A$, when we enlarge the radius to $R_B = \alpha R_A$ ($\alpha > 1$) where it still doesn't reach the saturation stage. And then, for the new condition B, we know the new electric field E_B is larger than E_A and we set $E_B = \beta E_A$ ($\beta > 1$). Now, the electric product is $E_B R_B = \alpha\beta E_A R_A$ under the fluence product $\Phi_B R_B = \alpha \Phi_A R_A$, of which relation is super-linear and doesn't accord with that in Fig. 2.

Moreover, it is revealed from Fig. 4 that the increase of the electric field strength with the radius could reach from 5 times to even an order, which means the scaling law in Ref. [28] might be less quantitative but more guiding for SGEMP protection. Meanwhile, a steady saturation is established when $R > 2.0$ m, and only at this time will the scaling law be more accurate and adoptable. According to Fig. 4, we establish the relation between electric field at the center E_1 and radius R under different heights h, and a more general logarithmic expression is as Eq. (11),

$$E_1 = \mathrm{A}(h) \times \log_{10}(R) + \mathrm{B}(h) \quad \left(\mathrm{kV \cdot m^{-1}}\right) \tag{11}$$

where A(h) and B(h) are two parameters as functions of the height of cylinder and will be introduced as follows.

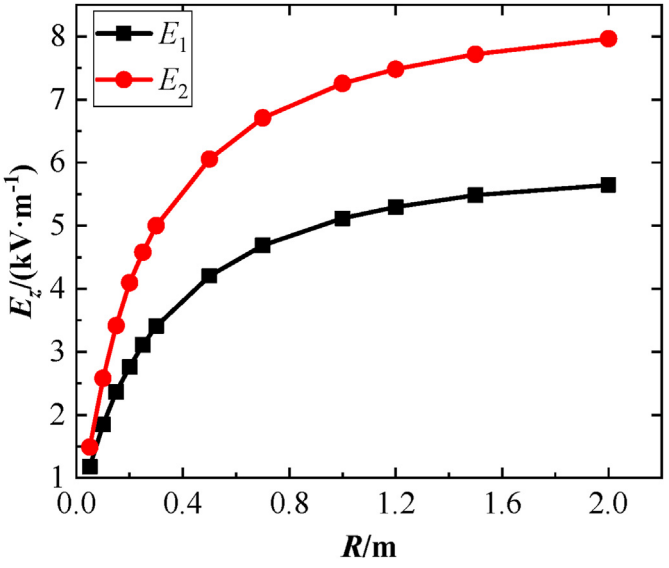

Fig. 4. Normal electric fields at the center point E_1 and at the edge E_2 on the emission surface. The height of the cylinder $h = 0.1$ m, and the energy fluence of the X-rays is $\Phi = 0.4$ J m^{-2}.

3.3. Influence of the height of the cylinder

The above content catches our eyes on how the radius affect the electric field and the scaling law. In this section, we are going to concentrate on the influence of the height of the cylinder, which was not mentioned before. Fig. 6 gives the relation between the electric fields (electric field at the center and electric field at the edge) mentioned before, and the height of the cylinder h, when the radius is fixed $R = 0.1$ m and the energy fluence of the X-rays is $\Phi = 0.4$ J m^{-2}. It is found that both electric fields will decrease with the increase of h. Even though the difference between the two electric fields is large with a short height, it becomes ignored as h grows large enough ($h > 2.0$ m in this model), where little edge-effect exists then. In order to obtain the quantitative relation between the two variates, we draw the curve that the two electric fields vary with $h^{-0.25}$ in Fig. 6(b). It is demonstrated that E_1 is nearly linear with $h^{-0.25}$, while E_2 behaves quadratically at the large height region, and luckily the small height condition could not be practical in reality. We show the relations of E_1 with $h^{-0.25}$ under four curves of different radii in Fig. 7, and they all seem to obey the same tendency (or slope) but different intercepts, and we fit the relation into Eq. (12),

$$E_1 = 0.4 \times h^{-0.25} + \mathrm{b}(R) \quad \left(\mathrm{kV \cdot m^{-1}}\right) \tag{12}$$

where b(R) is the intercept as a function of radius R.

Furthermore, it is attractive why the electric fields on the emission surface act as above. As we know, electric field is generated by the moving electrons, so how the electrons behave should be revealed. The pulsed electric current responses the variety of the electron density, and could be monitored by the magnetic field. Hence, two magnetic fields distributions of different heights ($h = 2.0$ m and $h = 0.1$ m) are displayed in Fig. 8. As for the long cylinder in Fig. 8(a), we can see the minimum contour line of the magnetic field could not reach the bottom of the cylinder but only on the side, while that line is able to cover the bottom of a short cylinder in Fig. 8(b). It means the difference between the maximum magnetic field at the top end and the bottom is larger in the long cylinder than in the short one. Table1 shows the specific magnetic field peaks at the two ends in the cylinder under different heights. We can discover that the fields at the top are going to increase with height while those at the bottom behave the exact opposite. The reason why they act like this is that the potential difference between the two ends could be larger with a longer height during the pulse acting time. So, the emission electrons could transport along the side of the cylinder more easily, leading to the larger current as well as the larger magnetic field. Hence, owing to the lower electron density at the top end, the electric fields there will decrease subsequently in accordance with expectation.

However, it is also demonstrated that there exists a steady saturation that the electric fields would not like to decrease infinitely when h is probably larger than 2.0 m. At this time, the differences among the fields on the emission surface are negligible as mentioned above and the scaling law in Ref. [28] will make sense.

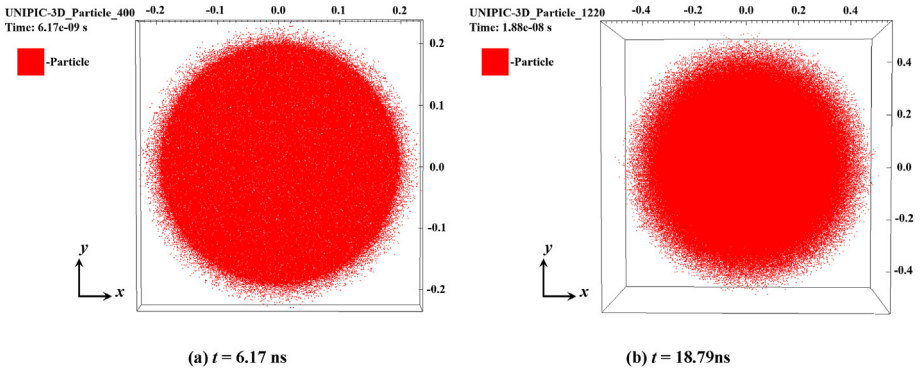

Fig. 5. Two-dimensional top view of the electron distribution above the emission surface at different times when $R = 0.2$ m, $h = 0.2$ m and $\phi = 0.4$ J m^{-2}. (a) An early stage that the emission surface of the cylinder is just carpeted with the injected electrons. (b) A middle stage that electrons have spread around to a larger scale parallel to the emission surface.

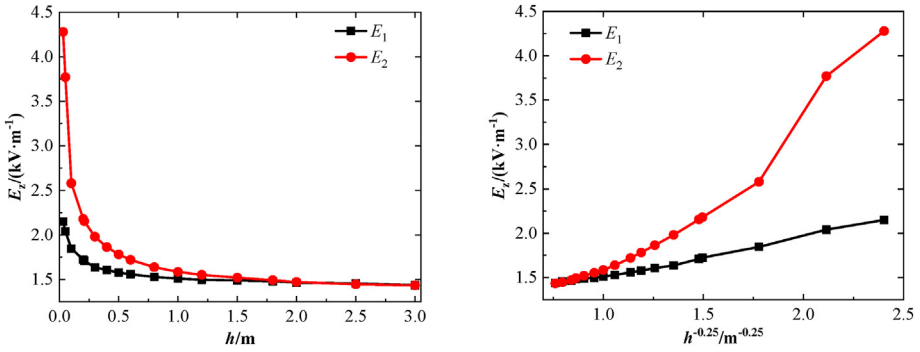

Fig. 6. Electric fields on the emission surface vs. the height of the cylinder h and $h^{-0.25}$ when the emission radius is fixed $R = 0.1$ m, and the energy fluence of the X-rays is $\Phi = 0.4$ J m^{-2}, where E_1 is at the center and E_2 is at the edge on the emission surface.

To make this paper more guiding with respect to verification of SGEMP code, it is necessary to give the exact relation between E_1, which represents the strength of the most electric field on the surface, and both the height h and radius R of the cylinder. Fig. 9 shows how the two parameters A and B in Eq. (11) vary with h and R, specifically. As we can see, the slope A(h) will rise sharply when h is smaller than 0.3 m, obeying an approximate logarithmic formula $A(h) = 0.30 \cdot \ln(h) + 3.5$, while it remains around 3.35 with neglectable fluctuation when h is larger than 0.3 m. For the intercept B(h), it always complies with the similar one-quarter law in Eq. (12) as $B(h) = 4.554 + 0.27 \cdot h^{-0.25}$. Now, through Eq. (11), one can get a rough electric field E_1 with higher reliability.

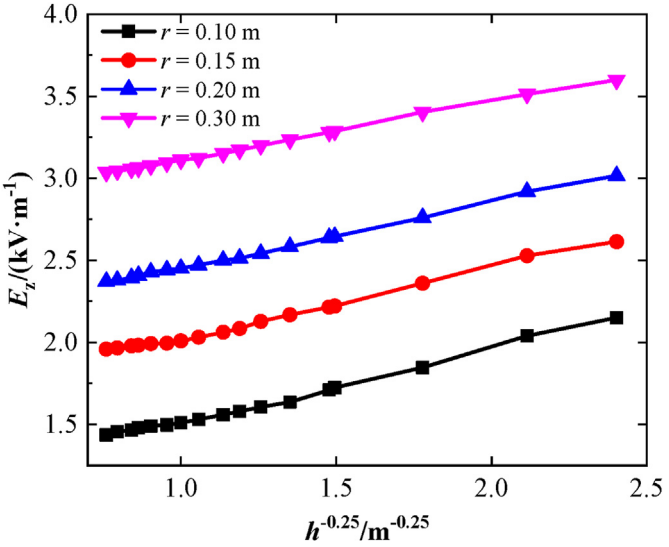

Fig. 7. Electric fields at center of the emission surface E_1 vs. $h^{-0.25}$ when cylinder radii are set $r = 0.10$ m, $r = 0.15$ m, $r = 0.20$ m and $r = 0.30$ m, respectively, and the fluence of the X-rays is $\Phi = 0.4$ J m^{-2}.

4. Conclusion

This paper has shown the impact of the geometrical parameters on the SGEMP response in the classical cylinder model that the electric field will be enlarged with radius but behave the opposite with that of height. Also, the influence of radius makes the scaling law in Ref. [28] inadaptable fatally. The differences of electric fields under different radii and heights could be huge that the electric field on a cylinder with larger radius or shorter height could be several times larger than that with a smaller radius or longer height. The particle and field distributions have been employed to explain how the parameters act on SGEMP responses. However, the saturation tells us that the electromagnetic fields will converge to some constant values so the scaling law will come back to its stage. The saturation usually occurs when the radius and height are both larger than 2.0 m. Lastly, we give a combination of logarithmic and minus one-quarter power law between the electric field at the center on the top surface E_1 and both the radius R and height h. The above findings will help us learn more about the influence of spacecraft size on SGEMP in detail, and will be useful for the wide application of the scaling law.

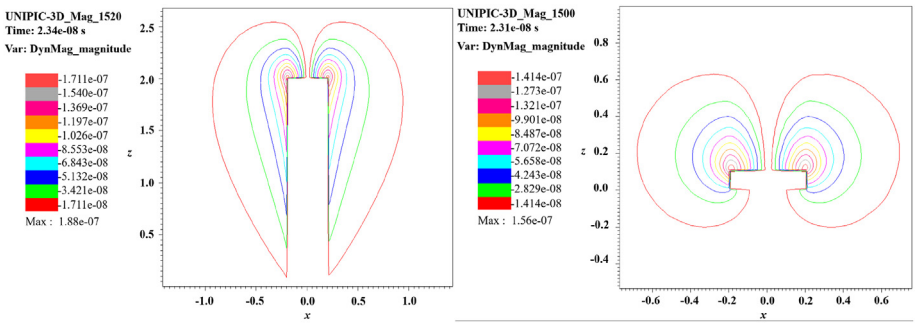

(a) $h = 2.0$ m (b) $h = 0.1$ m

Fig. 8. Two-dimensional side view of magnetic field distribution when the height of the cylinder (a) $h = 2.0$ m and (b) $h = 0.1$ m.

Table 1
Magnetic field peaks at different areas on the side wall of the cylindrical model vs. the height of the cylinder h, irradiated by X-ray of $\phi = 0.4$ J m^{-2}

Height of the cylinder h/m	Magnetic field peak on the side of the cylinder H/(A·m^{-1})	
	Top surface	Bottom surface
0.1	0.142	0.05
0.5	0.164	0.022
1.0	0.172	0.014
1.5	0.175	0.011
2.0	0.177	0.009
2.5	0.179	0.008

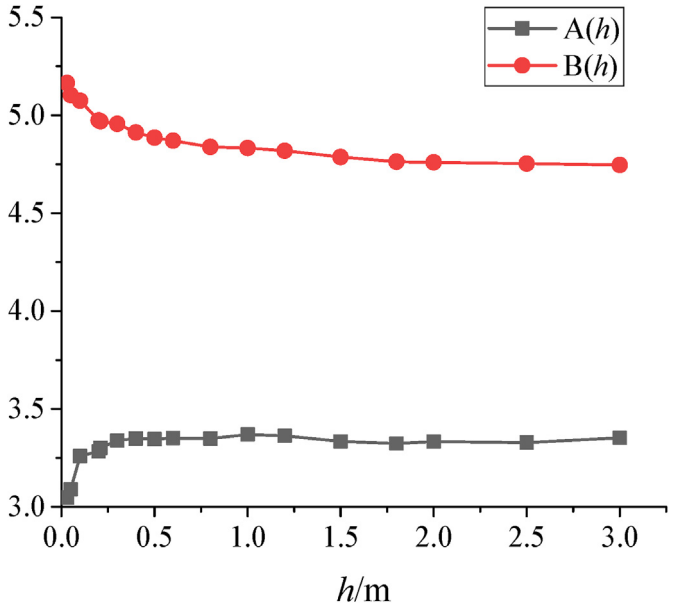

Fig. 9. Two parameters A(h) and B(h) vary with the height of cylinder h.

Data availability

The data that support the findings of this study are available from the corresponding author upon reasonable request.

Declaration of competing interest

The authors declare that they have no known competing financial interests or personal relationships that could have appeared to influence the work reported in this paper.

Acknowledgment

This work was supported by the National Key Research and Development Program of China under Grant No. 2020YFA0709800 and the National Natural Science Foundation of China under Grant No. 12105227.

References

[1] S. Glasstone, P.J. Dolan, in: The Effects of Nuclear Weapons, third ed., United States Department of Defense and the Energy Research and Development Administration, Washington, DC, 1977.
[2] M.J. Bernstein, K.W. Paschen, Forward and backward photoemission yields from metals at various X-ray angles of incidence, IEEE Trans. Nucl. Sci. 20 (1973) 111–116.
[3] A.J. Woods, W.E. Hobbs, E.P. Wenaas, Air effects on the external SGEMP responses of a cylinder, IEEE Trans. Nucl. Sci. 28 (1981) 4467–4478.
[4] M.J. Schmidt, Elementary external SGEMP model for system engineering design, IEEE Trans. Nucl. Sci. 32 (1985) 4295–4299.
[5] D.F. Higgins, Analytic calculations of the magnetic field produced by large SGEMP boundary layers, IEEE Trans. Nucl. Sci. 35 (1988) 1320–1323.
[6] E.P. Plomb, Analytical predictions of SGEMP response and comparisons with computer calculations, IEEE Trans. Nucl. Sci. 23 (1976) 1909–1915.
[7] R. Holland, Comparison of FDTD particle pushing and direct differencing of Boltzmann's equation for SGEMP problems, IEEE Trans. Electromagn C. 37 (1995) 433–442.
[8] R. Holland, A self-consistent two-dimensional EMP code for space-charge limiting and secondary emission, IEEE Trans. Nucl. 23 (1976) 1927–1932.
[9] J. Li, et al., Verification of numerical simulation model for SGEMP generated in Flash-II accelerator environment, Modern Appl. Phys. 7 (2016), 030503.
[10] L. Wang, et al., Analysis on numerical compute results of SGEMP effects simulation with DPF, Nucl. Electron. Detect. Technol. 19 (1999) 47–54.
[11] T.A. Tumolillo, J.P. Wondra, MEEC-3D : a computer code for self-consistent solution of the Maxwell-Lorentz equations in three dimensions, IEEE Trans. Nucl. Sci. 24 (1977) 2449–2455.
[12] W.F. Crevier, M.R. Bergstrom, Three-dimension SGEMP calculations using the modified fluid approach, IEEE Trans. Nucl. Sci. 28 (1981) 4221–4422.
[13] Z. Xu, C. Meng, Evaluation of cable SGEMP response using Monte Carlo and finite-difference time-domain methods, IEEE Trans. Nucl. Sci. 64 (2017) 2829–2839.
[14] J. Chen, C. Zeng, J. Deng, Z. Li, The secondary electron collection effect of biased printed circuit board traces in box IEMPs, IEEE Trans. Nucl. Sci. 69 (2022) 143–151.
[15] H. Zhang, Q. Zhou, H. Zhou, et al., Particle-in-cell simulations of low-pressure air plasma generated by pulsed x −rays, J. Appl. Phys. 130 (2021) 173303.
[16] B. Goplen, et al., User-configurable MAGIC for electromagnetic PIC calculations, Comput. Phys. Commun. 87 (1995) 54–86.
[17] J.P. Verboncoeur, et al., An object-oriented electromagnetic PIC code, Comput. Phys. Commun. 87 (1995) 199–211.
[18] J. Zhou, D. Liu, C. Liao, CHIPIC: an efficient code for electromagnetic PIC modeling and simulation, IEEE Trans. Plasma Sci. 37 (2009) 2002–2011.
[19] J. Wang, et al., Space charge limited current with distributed velocity of initial electrons in planar diode, Phys. Plasmas 28 (2021), 040702.
[20] J. Chen, et al., 2D planar PIC simulation of space charge limited current with geometrical parameters, varying temporal-profile and initial velocities, IEEE Access 10 (2022) 28499.
[21] L. Cai, et al., Two-dimensional simulation research of secondary electron emission avalanche discharge on vacuum insulator surface, Phys. Plasmas 22 (2015), 013502.
[22] J. Wang, et al., Three-dimensional parallel UNIPIC-3D code for simulations of

high-power microwave devices, Phys. Plasmas 17 (2010), 073107.
[23] J. Chen, et al., Simulation of SGEMP using particle–in-cell method based on conformal technique, IEEE Trans. Nucl. Sci. 66 (2019) 820–826.
[24] J. Chen, J. Wang, Z. Chen, Z. Ren, Calculation of characteristic time of space charge limited effect of SGEMP, IEEE Trans. Nucl. Sci. (2020) 818–822.
[25] J. Chen et al., Study of SGEMP field-coupling inside and outside reentrant cavity, IEEE Trans. Electromagn C., doi:10.1109/TEMC.2022.3153625.
[26] J. Chen, et al., Simulation of radiation environment and IEMP irradiated by low energy fluence X ray in cylindrical cavity, At. Energy Sci. Technol. 55 (2021) 360–368.
[27] J. Yao, Y. Zhao, H. Zhang, et al., Study of similarity rules for electromagnetic process in partially ionized plasmas, Phys. Plasmas 29 (2022), 012104.
[28] A.J. Woods, E.P. Wenaas, Scaling laws of SGEMP, IEEE Trans. Nucl. Sci. 23 (1976) 1903–1908.
[29] R. Stettner, The effect of various non-conducting gaps and surfaces on SGEMP and IEMP response, IEEE Trans. Nucl. Sci. 22 (1975) 2402–2407.
[30] H. Sun, Z. Dong, F. Zhang, Simulation analysis of external SGEMP effects of cylinder, J. Terahertz Sci. Electron. Inf. Technol. 14 (2016) 742–745.
[31] T.G. Jurgens, A. Taflove, K. Umashankar, T.G. Moore, Finite-difference time-domain modeling of curved surfaces, IEEE Trans. Antenn. Propag. 40 (1992) 357–366.
[32] D.N. Klochkov, A.N. Klochkov, Effect of the plasma electron motion on the development of Cherenkov instability in a waveguide, Plasma Phys. Rep. 28 (2002) 57–62.
[33] J.M. McMahon, S.K. Gray, G.C. Schatz, A discrete action principle for electrodynamics and the construction of explicit symplectic integrators for linear, non-dispersive media, J. Comput. Phys. 228 (2016) 3421–3432.
[34] J. Chen, Y. Tao, S. Niu, Calculation of electron emission parameters of SGEMP in cylinder cavity irradiated by X rays, Modern Appl. Phys. 11 (2020), 010501.